Polyhedron 155 (2018) 209–217

Contents lists available at ScienceDirect

Polyhedron

journal homepage: www.elsevier.com/locate/poly

Semiconducting, magnetic, luminescence properties and theoretical calculations of the tetra-azamacrocyclic compound: *trans*-Cr(cyclam)Cl_2] TCNQ

Juan Pablo León-Gómez [a], Rubén A. Toscano [b], Roberto Escudero [c], Francisco Morales [c], Enrique Camarillo [d], José M. Hernández [d], Héctor Murrieta [d], Christian Reber [e], Martha E. Sosa-Torres [a,*]

[a] Departamento de Química Inorgánica y Nuclear, Facultad de Química, Universidad Nacional Autónoma de México, Ciudad Universitaria, Cd. Mx., 04510, México
[b] Instituto de Química, Universidad Nacional Autónoma de México, Ciudad Universitaria, Cd. Mx., 04510, México
[c] Instituto de Investigaciones en Materiales, Universidad Nacional Autónoma de México, Ciudad Universitaria, Cd. Mx., 04510, México
[d] Instituto de Física, Universidad Nacional Autónoma de México, Ciudad Universitaria, Cd. Mx., 04510, México
[e] Département de Chimie, Université de Montréal, Montréal, QC H3C 3J7, Canada

ARTICLE INFO

Article history:
Received 22 February 2018
Accepted 31 July 2018
Available online 11 August 2018

Keywords:
$TCNQ^-$
Chromium(III)
Semiconductor
Luminescent
Magnetic

ABSTRACT

We report the new macrocyclic compound: *trans*-[Cr(*RSSR*-cyclam)Cl_2]TCNQ·H_2O (1), (where cyclam: 1,4,8,11-tetraazacyclotetradecane and TCNQ: 7,7,8,8-tetracyanoquinodimethane). Its 3D structure showed π-π interactions between the $TCNQ^-$ moieties with alternating distances (3.24 and 3.87 Å). **1** exhibited an electric conductivity, $\sigma = 1.94 \times 10^{-5}$ Scm^{-1} at 300 K and a band-gap of 0.53 eV in the range of a semiconductor. Its magnetic behavior is of a typical Curie–Weiss paramagnet with an antiferromagnetic coupling ($\theta = -15$ K). The measured magnetic moment, $\mu_{exp} = 3.84$ B. M. at room temperature is lower than the expected, $\mu_{calc} = 4.86$ B. M. (only spin) for a d^3 octahedral chromium (III) and an anionic radical $TCNQ^-$; this is explained by the presence of diamagnetic dimers of $TCNQ^-$ in the crystal packing. **1** shows photoluminescence at low temperature from 80-17 K. Finally, by using DFT calculations, it was possible to assign van der Waals (CH–π, Cl–π) interactions and N–H hydrogen bonding, which are likely determining the observed antiferromagnetism. The calculations also allowed us to verify the presence of diamagnetic dimers in the crystal packing, formed by strong π–π interactions of TCNQ-entities.

1. Introduction

The theoretical as well as the experimental research focused on functional molecular materials has increased notably in the last decades. The interest, is based on the specific properties and advantages of these new materials compared to conventional inorganic materials, like lightness, synthesis at relatively low temperatures, flexibility, multifunctionality, among others [1]. The study of these systems is also attractive in view of their potential technological applications like: spintronics, molecular sensors, data storage, quantum processing of information, etc. [2]. Besides, the synthesis of molecules that combine two or three functional properties, either magnetic, photophysics, or electric, represent a great challenge for many scientists.

The relevance of these compounds for materials sciences is due mainly to the almost unlimited modulation of their physical properties by conventional methods in chemical synthesis through soft routes, from organic, coordination to supramolecular chemistry [3]. In this field, coordination compounds with properties of technological interest are already known [4].

The combination of two or more functional properties in a given compound is achieved through the appropriate selection of the molecules and/or ions that already have those properties. The organic radicals have been an important source in the design of multifunctional materials based on molecules [5]. In this way, the coordination of the functional molecule to a metal ion leads to an increase of its properties compared to the individual molecules. One of the most used organic radical in the design of materials that combine magnetic and electric properties has been the anion $TCNQ^-$ [6]. Some compounds based on TCNQ that present semi and conductive properties are AgTCNQ, TlTCNQ, CuTCNQ, MnTCNQ4 [7]. AgTCNQ and CuTCNQ have also optical properties that make them suitable to be used as optical switches [8]. Additionally, the organic metal TTF-TCNQ presents magnetoresistance [9]. The iron complexes, [Fe(abpt)$_2$(TCNQ)$_2$], [Fe(acpa)$_2$]

* Corresponding author.
E-mail address: mest@unam.mx (M.E. Sosa-Torres).

https://doi.org/10.1016/j.poly.2018.07.052
0277-5387/

(TCNQ) and $[Fe(HC(pz)_3)_2](TCNQ)_3$ present the phenomenon of spin-crossover, [10]. Historically, compounds formed with TCNQ were known by presenting high electric conductivities that could be explained by their π-π stacking among the $TCNQ^-$ units [11].

On the other hand, up to date, few compounds with chromium and TCNQ in their structure are known. In the 90's, the decametylchromocene: $[Cr(C_5(CH_3)_5)_2][TCNQ]$ was reported as a massive ferromagnet with a T_c = 3.1 K [12]. The crystalline structure of this compound, is an alternate packed one, between the donor chromium and the acceptor $(TCNQ^-)$,...D + A − D + A−..., which magnetic properties could be explained due to the CT configuration mixing mechanism. Additionally, some compounds based on TCNQ have shown ferromagnetism. such as $[Mn(C_5(CH_3)_5)_2)]$TCNQ [13], $(NMe_4TCNQ) \cdot ½TCNQ$ [14], $[Fe(C_5(CH_3)_5)_2][TCNQ]$ [15], $(CsTCNQ) \cdot ½TCNQ$ [14] and $V[TCNQ]_2$ [16]. The first reports on compounds formed by the chromium and TCNQ, the $[(C_6H_5CH_3)_2Cr]^+(C_{12}H_4N_4)^-$ $(C_{12}H_4N_4)$, indicated that they were semiconductors, besides in their crystalline packing, it was found that the TCNQ units were stacked into an infinite array [17]. More recently, the group of J. Nishijo, has reported the compounds: [Cr(cyclam)(C≡C-MeEDT-TTF)$_2$](TCNQ)$_3$ (MeEDT-TTF = 5-methyl-4′,5′-ethilenedithiotetratiafulvalen) and [Cr(cyclam)(C≡C-6-methoxynaphtalen)$_2$](TCNQ)$_n$ (1,2-dichloroethane) (n = 1, 2) NaphOMe = 6-methoxynaphtalen, n = 1, 2), which presented ferro and ferrimagnetism [18]. Additionally, it should be mentioned that the dichlorocyclamchromium(III) X based compounds (X = $ZnCl_4$, $CrCN_6$, Cl) exhibit luminescence [19]. Here we describe the synthesis, characterization and semiconducting, magnetic and luminescence properties, as well as DFT theoretical calculations of the new macrocyclic chromium compound *trans*-[Cr(Cyclam)Cl_2]TCNQ·H_2O.

2. Experimental

2.1. Materials

All chemicals were from Sigma-Aldrich, without further purification.

2.2. Physical measurements

Fourier transform infrared reflectance spectra over the range 4000–400 cm^{-1} of the complexes were obtained on a Perkin–Elmer 599-B instrument. Raman spectra were measured on a Renishaw Invia microscope spectrometer using an argon ion laser with an excitation wavelength of 514.5 nm and a Linkam liquid nitrogen cryostat to control the sample temperature. Electronic absorption spectra were measured on a diluted sample in a pellet with KBr on a Cary – 5E Varian spectrometer over the range 40,000–4,000 cm^{-1} in diffuse reflectance mode. The photoluminiscence spectra were recorded with an excitation wavelength of an Ar laser (λ = 514 nm, 100 mW) at 80 K and with a YAG-Nd laser (λ_{exc} = 532 - nm, 500 mW) and (λ_{exc} = 650 nm, 1000 mW) at 17 K on sample pellets mounted on a copper sample holder of an Air Products helium closed cycle cryostat and the resultant signals were averaged and saved in an Infinium 500 MHz Hewlett–Packard Digital Oscilloscope. Elemental analyses C, H and N were carried out in a Perkin–Elmer 2400, using cystine as standard. EPR spectra were recorded on polycrystalline samples at room temperature with a Bruker Elexsys E500 spectrometer using the X-band (9.45 GHz) microwave frequency operating at 100 kHz. The g values were determined by measuring the magnetic field and the microwave frequency. The magnetic susceptibility measurements were obtained by using a Gouy balance at 300 K which was calibrated with $Hg[Co(SCN)_4]$ as standard. Experimental effective magnetic moments were obtained using the expression: $\mu_{exp} = 2.83\sqrt{\chi M^{cd} T}$ B. M. and compared with the calculated effective magnetic moment, only spin, $\mu_{calc} = 2\sqrt{S(S+1)}$ B. M. Magnetic susceptibility versus temperature was measured in the range of 2–300 K and carried out using a MPMS SQUID magnetometer. Isothermal magnetization studies as a function of field strength (−5 – 5 T) were performed at 2 K. The magnetic measurements were performed on microcrystalline powdered sample and corrected for the diamagnetism using Pascal's constants [20]. The electrical resistance was obtained as a function of temperature (254–298) K by using a two-pronged measurement approach on a sample bar of 1 mm^2 - × 1 cm. The readings of the electrical resistance were done through a *Hewlett Packard* model 3478 A multimeter and the temperature was taken with a *LakeShore* model 330 controler.

2.3. Synthesis of trans-[Cr(cyclam)Cl_2]TCNQ·H_2O

trans-[Cr(cyclam)Cl_2]Cl (0.3587 g, 1 mmol) (prepared according to Sosa and Tobe [19c]) was dissolved in the minimum amount of water and some drops of a hot saturated solution of LiOH were added till the solution changed from pink to a light orange colour. Separately, (0.4222 g, 2 mmol) of LiTCNQ (obtained according to the published method [6e]) were dissolved in 200 mL of a mixture of acetonitrile/methanol (2:1) and added to the previous solution, under N_2. The resulting mixture was under reflux for 4 h. The final solution was set aside for several days, until deep purple crystals were formed. These crystals were filtered and washed with cold water and dried to air (Yield = 65%). Calculated elemental analysis for **1**, $CrC_{22}H_{30}N_8OCl_2$, C:48.45, H:5.54, N:20.54 % coincided well with the experimental analysis found for 1: C: 49.68, H: 5.18, N: 20.63 %.

2.4. Crystal structure determination

The crystal evaluation and data collection were performed at 150 K on a Bruker Smart Apex CCD diffractometer with MoKα (λ = 0.71073 Å) radiation. Deep-blue crystals of $\{[C_{10}H_{24}Cl_2CrN_4]^+, [C_{12}H_4N_4]^-\}\cdot H_2O$ appeared as needles, a sample with approximate dimensions 0.057 × 0.148 × 0.456 mm, proved to be a two-component twin with a 28.5% second component contribution. The twin components are related by a 179.9° rotation about reciprocal axis [1 0 2]. Frames were integrated using the Bruker SAINT software. Experimental data were corrected for Lorentz, polarization, and absorption effects; for the latter, the multiscan method was employed using Bruker TWINABS software. The structure was solved as dual space approach as implemented in SHELXT and difference Fourier maps as embedded in the SHELXL-2016/6 software running under SHELXLE [21]. Hydrogen atom positions were determined employing difference Fourier maps; these were later used as a starting point for the refinement with the following constraints: N···H distances at same distance value (SADI) and isotropic displacement parameters 1.2 the U_{eq} of the corresponding parent N-atom and the O–H bonds distances make similar (SADI) with the U_{iso} refined freely. The final refined positions of hydrogen atoms defined a reasonable hydrogen-bond network. Crystallographic data have been deposited at the Cambridge Crystallographic Data Center as supplementary material number CCDC 1547475. Copies of the data can be obtained free of charge on application to CCDC, 12 Union Road, Cambridge CB2 1EZ, UK. E-mail: deposit@ccdc.cam.ac.uk.

2.5. Computational method

To evaluate the contribution of the intermolecular interactions on magnetic properties presented by this mononuclear compound **1**, a Density Functional Theory (DFT) study was performed. Using

the quantum chemistry software GAUSSIAN-09 [22], all-electron calculations were done at the B3LYP/6-311+G(d,p) level of theory [23].

3. Results and discussion

3.1. Synthesis and characterization

The reaction between *trans*-[Cr(cyclam)Cl_2)Cl and LiTCNQ produced a very dark purple solution which was set aside for several days, until deep purple crystals were formed. The I.R. (ν_{max}, cm^{-1}, vs: very strong, s: strong, m: medium and w: weak intensities) of the product showed bands at 3535m, [ν(HOH)], 3209s [ν(NH)], 2945w, 2932w, 2910 w, 2878w [ν(CH)], 2175vs, 2166vs, 2157s cm^{-1} [ν(CN)], 1575s, 1505 m cm^{-1} [ν(C=C)], 1466m, 1451w, 1425w cm^{-1} [δasym(C-H2)], 1359–1298 m cm-1 [δsym (C-H2)] and 823w cm^{-1} [δar(C–H)]. Raman bands ($\lambda_{max.}$ cm^{-1}, Stokes, measured at 80 K) were observed at 3210w, 2950w (broad), 2214s, 1601vs, 1520w, 1430w, 1330m, 1275m, 1175m, 1005w, 960w, 344w, 230w. The frequencies of Raman bands at 3210, 2950, 1430, 1330, 1175, 1005 and 960 are consistent with the frequencies of vibrational modes of **1** observed in the IR.

3.2. Single-crystal X-ray diffraction

The crystal data and the structure refinement of compound **1** is listed in Table 1. The structure of the title compound consists of a *trans* dichloro cyclam chromium complex cation [Cr(cyclam) Cl_2]$^+$, $TCNQ^-$ anion and a water solvent molecule. The macrocyclic skeleton adopts the most stable *trans*-III conformation [24]. The diffraction study revealed that chromium(III) is in a distorted octahedral environment with axial bonds elongated with respect to the equatorial ones. The chromium(III) ion lies in the center (−0.0108(11)Å) of a four-nitrogen plane (N1: 2.048 Å, N11: 2.050 Å, N8: 2.063 Å and N4: 2.067 Å) (Rms = 0.0146 Å) and its coordination environment is completed by two chlorine atoms in the apical positions (Cl1: −2.3384(12) Å and Cl2: 2.3187(12) Å). The $TCNQ^-$ anion is essentially planar (Rms deviation over all atoms = 0.0551 Å) making an angle to previous plane = 50.477(38)°, shown in Fig. 1, Table 3.

Table 1
Crystal data and structure refinement for *trans*-[Cr(cyclam)Cl_2]TCNQ·H_2O.

Empirical formula	$C_{22}H_{30}Cl_2CrN_8O$	
Formula weight	545.44	
Crystal system	monoclinic	
Space group	$P2_1/c$	
Unit cell dimensions		
	a = 13.988 Å	α = 90°
	b = 6.486 Å	β = 99.082°
	c = 28.008 Å	γ = 90°
V	2509.2 $Å^3$	
Z	4	
D_{calc}	1.444 Mg/m^3	
Absorption coefficient	0.701 mm^{-1}	
T	123 K	
F(0 0 0)	1136	
θ range	1.912–27.480°	
Index ranges	$-18 \le h \le 17$, $0 \le k \le 8$, $0 \le l \le 36$	
Reflections collected	5732	
Independent reflections	5732 [R_{int} = 0.0523]	
Completeness to θ = 25.242°	99.9%	
Max. and min. transmission	0.9611 and 0.7401	
Data/restrains/parameters	5732/7/328	
Goodness-of-fit on F^2	1.086	
Final R indices [$I > 2\sigma(I)$]	R_1 = 0.0389, wR_2 = 0.0806	
R indices (all data)	R_1 = 0.0481, wR_2 = 0.0855	
Largest diff. peak and hole (e $Å^3$)	0.636 a nd −0.357	

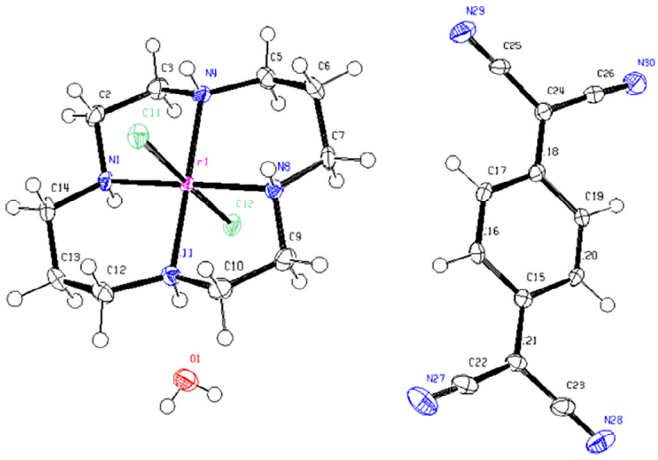

Fig. 1. ORTEP drawing of *trans*-[Cr(cyclam)Cl_2]TCNQ·H_2O with thermal ellipsoids on the 50% probability level.

In the crystal packing, neighboring molecules of the cation complex are connected *via* strong hydrogen bonds (2.49 Å) between protonated amine groups (N1 and N8) and chlorine atoms, forming the structural motif of eight-membered rings and infinite chains along the ***b*** direction. Along the same direction the aromatic rings of $TCNQ^-$ anions stack into columns with centroid distances of 3.8711(14)[1 − *x*, 1 − *y*, −*z*] and 3.2419(14)[1 − *x*, −y, −*z*] Å above and below. These chains and columns are interconnected through H-bonds by intermediacy of the water solvent [O1… N27, O1…N30] and direct interaction between the cations and anions [N4…N28] [Fig. 2, Table 2]. The stacking between TCNQ units shows strong π–π interactions (3.8711 and 3.2419 Å) [Fig. 3], as well as CH–π interactions with the *trans*-[Cr(cyclam)Cl_2]$^+$ [Fig. 4].

3.3. Electronic spectra

3.3.1. Absorption

The UV–Vis spectrum (298 K) of *trans*-[Cr(cyclam)Cl_2]TCNQ·H_2-O in the solid state exhibited two broad bands, at 370, and at 589 nm [Fig. 5]. A further analysis by subtracting the base line of such spectrum produced a well-defined absorption bands at λ_{max} = 370 and λ_{max} = 589 nm. (black line experimental spectrum in Fig. 6). Then, it was deconvoluted and four overlapping bands were obtained [Fig. 6]. The intense bands at 368 and 671 nm (green line) correspond to allowed intramolecular transitions of $TCNQ^-$. The band at higher energy is assigned to the $\pi^2 1\pi^{*1}$ ($^2B_{2g}$) → $\pi^2 2\pi^{*1}$ (2^2B_{3u}) transition which can be interpreted as a HOMO–LUMO transition of TCNQ, while the band at 671 nm is assigned to the $\pi^2 1\pi^{*1}$ ($^2B_{2g}$) → $\pi^1 1\pi^{*2}$ (1^2B_{3u}) transition. Additionally, the peaks at 421 ($^4A_{2g} \rightarrow {}^4T_{1g}$) and 586 ($^4A_{2g} \rightarrow {}^4T_{2g}$) nm. (pink line) are typical of the electronic transitions of chromium(III) compounds in an octahedral field, which are Laporte forbidden and spin allowed. Their maxima are at slightly longer wavelengths than the values of 412 and 567 nm reported for *trans*-[Cr(cyclam)Cl_2]Cl in the solid state [19b] and also than the values of 406 and 542 nm reported for *trans*-[Cr(cyclam)Cl_2]$^+$ in aqueous solution [25].

3.3.2. Luminescence

Pellets obtained from the solid samples of **1** were excited with an Ar laser at wavelengths, λ_{exc} = 514 nm, 100 mW at 80 K and at λ_{exc} = 532 nm, 500 mW and λ_{exc} = 650 nm, 1000 mW at 17 K. At 80 K, the emission spectrum shows a weak broad band centered at 840 nm, most likely quenched at room temperature, this band becomes broader and more intense as the temperature decreases at 17 K (see Fig. 7). This emission band is shifted to a lower energy

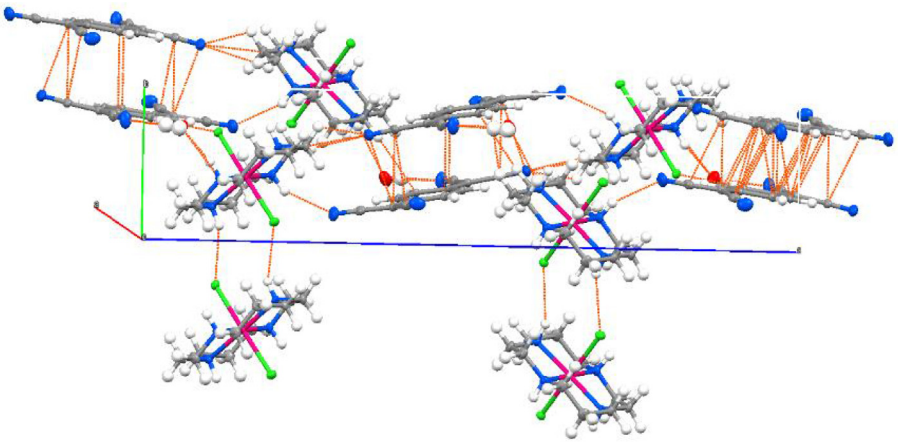

Fig. 2. Hydrogen bonding and van der Waals interactions found in *trans*-[Cr(*cyclam*)Cl_2]TCNQ.

Table 2
Hydrogen bonds for *trans*-[Cr(cyclam)Cl_2]TCNQ·H_2O [Å and °].

D–H...A	d(D–H)	d(H...A)	(DHA)
O(1)–H(1A)...N(27)#1	0.71	2.28	154
O(1)–H(!B)...N(30)#2	0.71	2.26	159
N(1)–H(1)...Cl(1)#3	0.851	2.59	146
C(3)–H(3A)...Cl(2)	0.99	2.93	109.7
C(3)–H(3B)...N(29)#4			
N(4)–H(4)...N(28)#5	0.856	2.36	150
N(8)–H(8)...Cl(2)#6			
C(10)–H(10A)...N(30)#7			
C(10)–H(10B)...O(1)#6			
N(11)–H(11)...O(1)			
C(12)–H(12A)...Cl(1)			

Symmetry transformations used to generate equivalent atoms: #1 $-x, -y+1, -z$ #2 $-x+1, -y+1, -z$ #3 $x, y+1, z$ #4 $-x+1, y+1,/2, -z+1/2$ #6 $x, y-1, z$ #7 $x-1, y,z$.

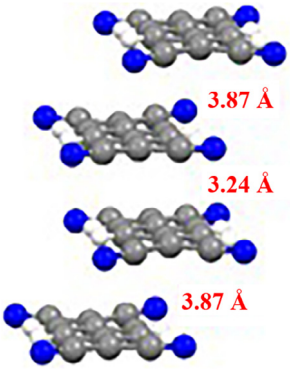

Fig. 3. π–π stacking among $TCNQ^-$ units along *b* axis showing alternating distances.

Table 3
Selected bond lengths [Å] and angles [°] for *trans*-[Cr(cyclam)Cl_2]TCNQ·H_2O.

Bond	Length (Å)		
Cr(1)–N(1)	2.048	C(10)–N(11)	1.497
Cr(1)–N(11)	2.050	N((11)–C(12)	1.482
Cr(1)–N(8)	2.063	C(12)–C(13)	1.522
Cr(1)–N(4)	2.067	C(13)–C(14)	1.525
Cr(1)–Cl(1)	2.330	C(15)–C(21)	1.412
Cr(1)–Cl(2)	2.331	C(15)–C(20)	1.424
O(1)–H(1A)	0.71	C(15)–C(16)	1.428
O(1)–H(1B)	0.71	C(16)–C(17)	1.359
Angles(°)			
N(1)–Cr(1)–N(11)	93.85	C(3)–N(4)–Cr(1)	106.24
N(1)–Cr(1)–N(8)	178.37	N(4)–C(5)–C(6)	112.6
N(11)–Cr(1)–N(8)	85.34	C(5)–C(6)–C(7)	116.5
N(1)–Cr(1)–N(4)	85.25	N(8)–C(7)–C(6)	112.31
N(11)–Cr(1)–N(4)	179.07	C(7)–N(8)–C(9)	114.5
N(8)–Cr(1)–N(4)	95.57	C(7)–N(8)–Cr(1)	116.16
N(1)–Cr(1)–Cl(1)	92.53	C(9)–N(8)–Cr(1)	106.53
N(11)–Cr(1)–Cl(1)	91.64	N(8)–C(9)–C(10)	108.2
N(8)–Cr(1)–Cl(1)	88.91	N(11)–C(10)–C(9)	108.4
N(4)–Cr(1)–Cl(1)	88.18	C(12)–N(11)–C(10)	113.2
N(1)–Cr(1)–Cl(2)	87.07	C(12)–N(11)–Cr(1)	116.96
N(11)–Cr(1)–Cl(2)	90.08	C(10)–N(11)–Cr(1)	106.66
N(8)–Cr(1)–Cl(2)	91.51	N(11)–C(12)–C(13)	111.8
N(4)–Cr(1)–Cl(2)	90.09	C(12)–C(13)–C(14)	116.1
Cl(1)–Cr(1)–Cl(2)	178.26	N(1)–C(14)–C(13)	112.02

compared to the lowest energy absorption band (586 nm, Fig. 5) attributed to Cr(III) in *trans*-[Cr(cyclam)Cl_2]TCNQ·H_2O, showing the expected Stokes shift. On the other hand, the emission spectrum of the reactant *trans*-[Cr(cyclam)Cl_2]Cl (see Fig. 7) shows four sharp peaks at 681, 694, 708 and 721 nm [19b], attributed to the emissions from $^2T_{1g}$ and ^2E_g energy levels of the tetragonal distorted *trans*-[Cr(cyclamCl_2]Cl. There is a clear difference when comparing the above mentioned sharp bands with the emission broad band centered at 840 nm in **1**, indicating that the latter emission originates from a different excited state, namely from $^4T_{2g} \rightarrow {}^4A_{2g}$. This is exceptional but consistent with the longer-wavelength maximum of the $^4T_{2g}$ absorption band. The sharp bands characteristic of the forbidden transitions $^2T_{1g} \rightarrow {}^4A_{2g}$ and $^2E_g \rightarrow {}^4A_{2g}$ are not found in the emission spectrum of **1** under these conditions.

3.4. Magnetic properties

The magnetic susceptibility at 300 K corrected for diamagnetism [20], was used to calculate the magnetic moment for *trans*-[Cr(cyclam)Cl_2]TCNQ·H_2O, μ_{exp} = 3.84 B. M., which is lower than the expected for a d^3 in chromium (III) and a radical $TCNQ^-$, μ_{cal} = 4.86 B. M. (only spin) and very close to the μ_{exp} value of 3.88 B. M. for a chromium(III) complex. The magnetic susceptibility was also studied as a function of temperature (2–300 K) [Fig. 8]. The obtained plot showed a typical Curie-Weiss behavior, no magnetic transition was observed in this range of temperature.

From the linear plot $1/\chi$ *versus* T in the range of 2–300 K (Fig. 8 insert), a Weiss constant (θ) of −15.38 K was obtained indicating a weak antiferromagnetic ordering in the compound. The obtained Curie constant, 1.898 cm^3 K/mole was used to calculate a total spin of $S = 3/2$. The plot of μ_{exp} *versus T* is linear at high temperatures and at approximately 40 K, a sudden fall in the magnetic moment,

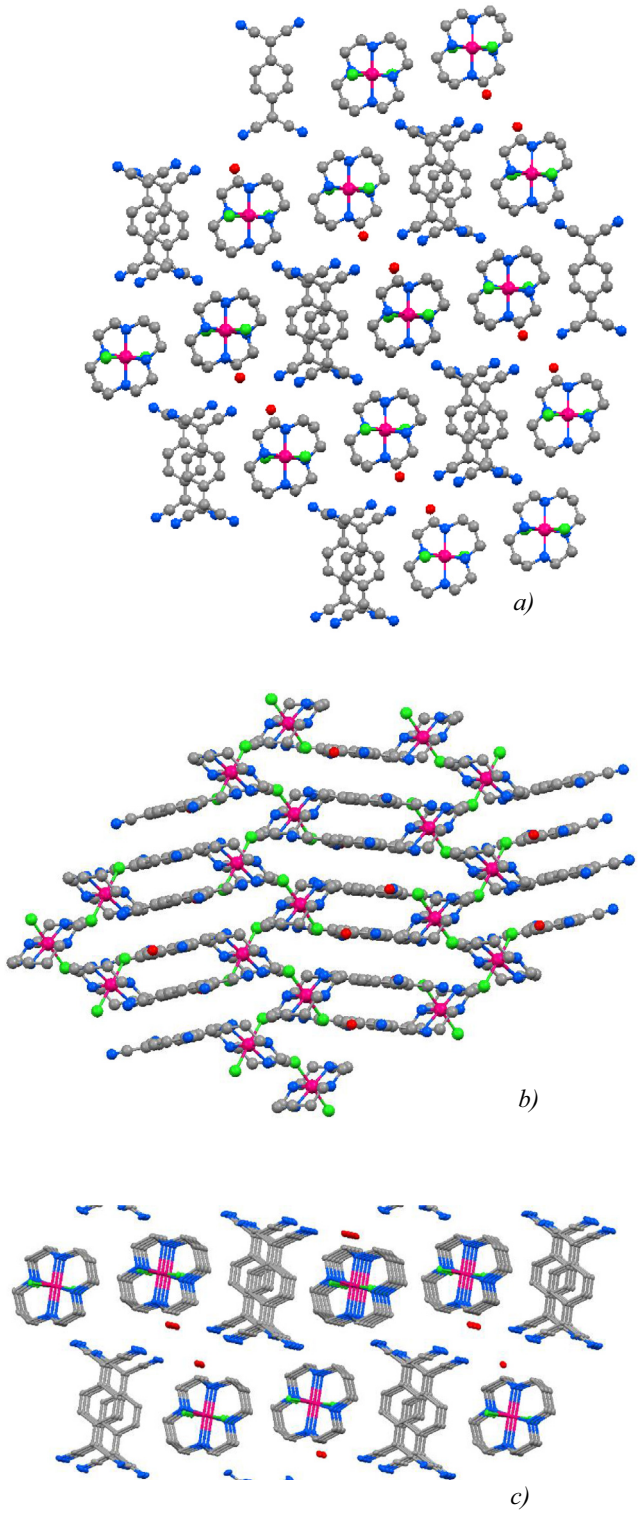

Fig. 4. View in direction of (a) axis *b* and (b) axis *a*, (c) perspective view in the crystal structure of *trans*-[Cr(cyclam)Cl_2]TCNQ·H_2O. Hydrogens are omitted for clarity.

characteristic of an antiferromagnetic material [Fig. 9]. The expected value for the magnetic moment at high temperatures is greater than that observed for **1**. Finally, from the graph of magnetization as a function of the applied magnetic field at low temperature showed a linear curve, characteristic of common paramagnets [Fig. 10].

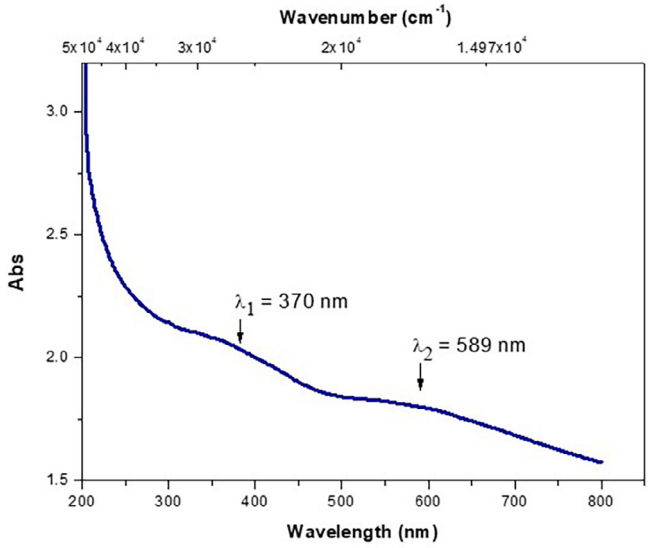

Fig. 5. Solid UV–Vis. experimental spectrum of **1**.

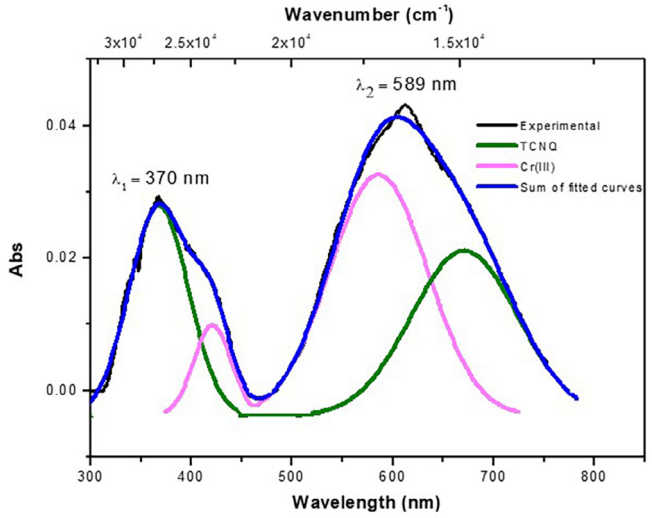

Fig. 6. Deconvoluted experimental UV–Vis spectrum of **1** showing the bands for Cr^{3+} and $TCNQ^{-}$.

3.5. EPR spectrum

The EPR of **1** (powder), was obtained at X-Band at 298 K and frequency = 9.86715 GHz. [Fig. 11]. It showed an isotropic signal at $g = 2.025$ and line width of 684 Gauss, typical of Cr(III) compounds. The radical from $TCNQ^{-}$ was not observed, these results are consistent with the previous discussion.

3.6. Electrical properties

The electric resistance *versus* T of **1** was measured from 298 to 254 K. The measured values were multiplied by area/length of the pellet in order to get the resistivity (ρ). The conductivity ($\sigma = 1/\rho$) *versus* T of **1**, increases exponentially as the temperature increases [Fig. 12]. This behavior is observed in semiconducting materials [26]. Thus, the electric conductivity found at 298 K was 1.941×10^{-5} Scm^{-1}, this value it is also in the range of the semiconductors. (for example, Si: 5×10^{-6}, Ge: 2×10^{-2}, KTCNQ: 5×10^{-3} Scm^{-1}).

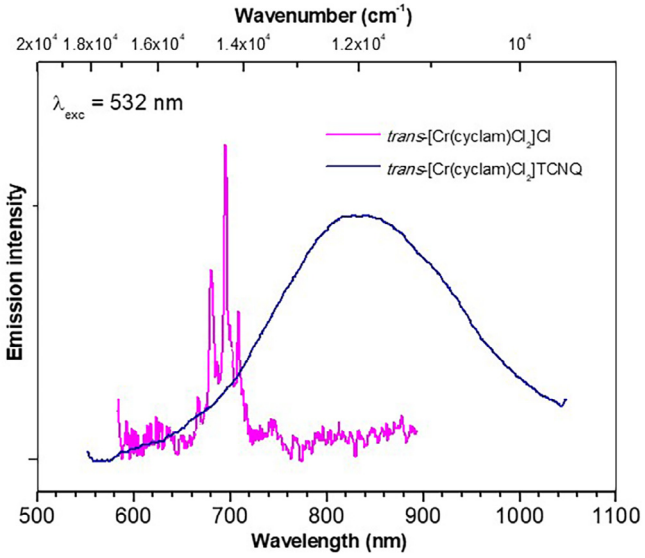

Fig. 7. Emission spectra at 17 K of *trans*-[Cr(cylam)Cl_2]Cl and *trans*-[Cr(cylam)Cl_2] TCNQ in the solid state showing emission bands of chromium (III).

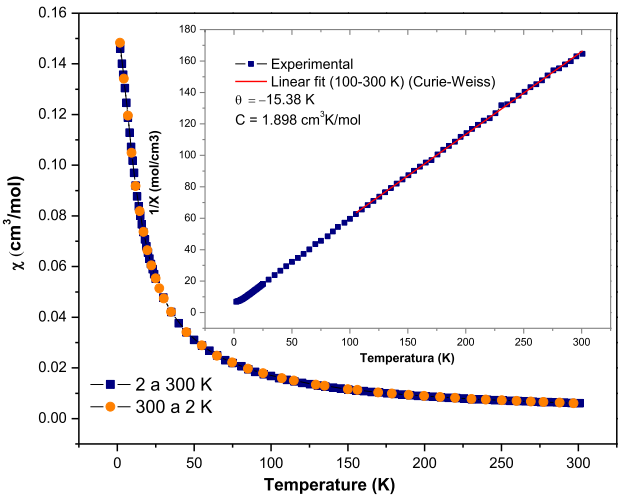

Fig. 8. Magnetic susceptibility of **1** as a function of temperature.

When the ln(σ) was plotted against $1/T$, a straight line with a negative slope was obtained [Fig. 12 insert]. This curve was adjusted with the electric conductivity of an intrinsic semiconductor model and can be written as:

$$\sigma = 2e\mu_p(b+1)\left(\frac{2\pi\left(m_p^* m_n^*\right)^{\frac{1}{2}}kT}{h^2}\right)^{\frac{3}{2}} e^{-\frac{E_g}{2kT}} \quad (1)$$

Under these conditions, the term $T^{3/2}$ in Eq. (1) is negligible, as it varies slowly compared to the exponential term ($E_g \gg kT$). Then, E_g, was evaluated as 0.53 eV, being the value of the band gap for **1** [Fig. 13] which lies within the magnitude of semiconductors (Si: 1.11 eV, Ge: 0.66 eV). The semiconductor behavior of this compound can be visualized by the movement of the electrons along the *b* axis which presents π–π interactions among the $TCNQ^-$ radicals.

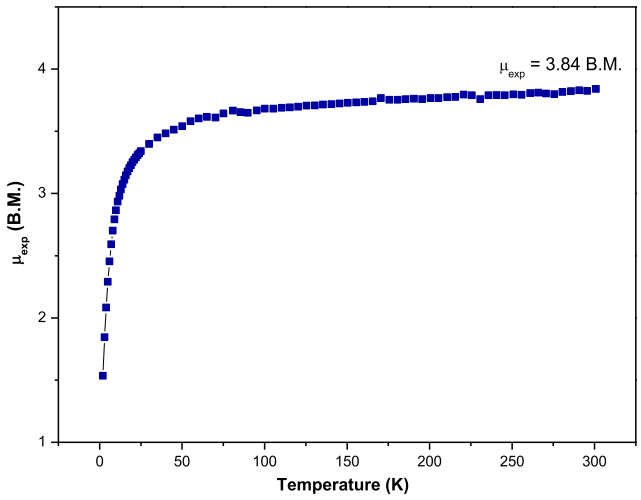

Fig. 9. Effective magnetic moment *vs* temperature.

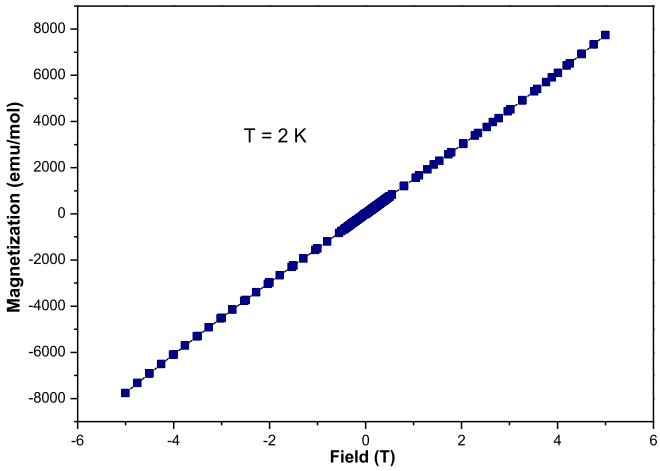

Fig. 10. Curve of magnetization as a function of the applied magnetic field at 2 K.

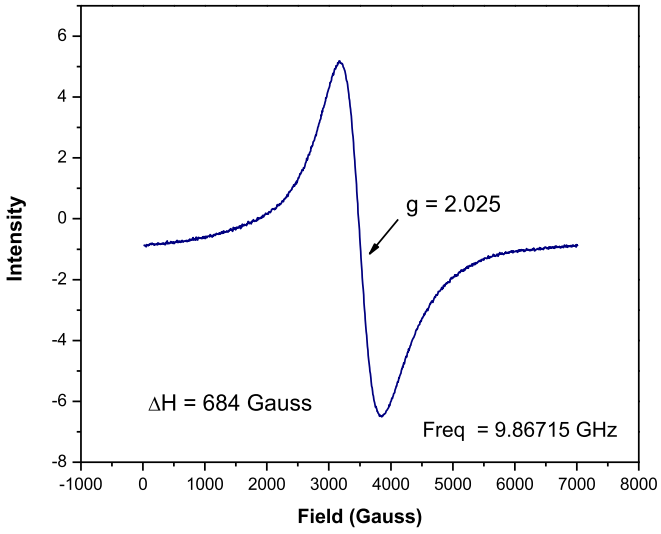

Fig. 11. X-band EPR spectrum at 298 K for polycrystalline sample of **1**.

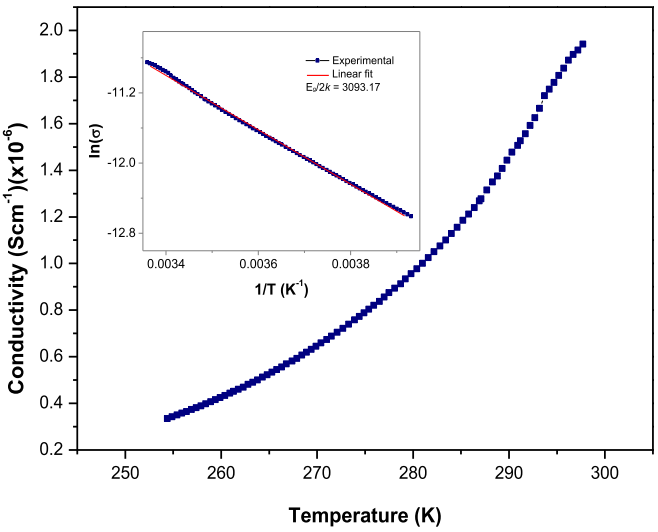

Fig. 12. Electrical conductivity as a function of temperature for **1**.

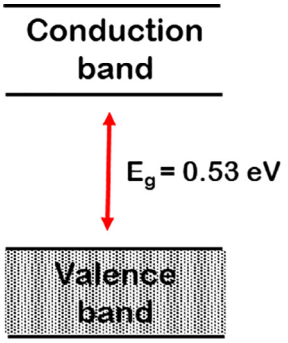

Fig. 13. Band-gap found for **1**.

Interestingly, the compound Tl(TCNQ) [7b], in its two crystalline phases, (Tl(TCNQ)) I and Tl(TCNQ) II, exhibit very different electric conductivities, namely 2.4×10^{-4} for I and 5.4×10^{-1} Scm^{-1} for II. For the phase II with the higher conductivity, the distances between the TCNQ molecules along the stacking showed equal distances (3.22 Å), while those found in the phase I, had different distances (3.16 and 3.35 Å), the latter, reflects a partial dimerization leading to the formation of a spin-Peierls insulator state and a relatively low conductivity.

In our molecule, **1**, we also found, that the distances between TCNQ$^-$ molecules are different (3.24 and 3.87 Å), along the b axis, suggesting the formation of dimers between the TCNQ$^-$ radicals and due to its relatively low conductivity (1.941×10^{-5} Scm^{-1}) it is likely that the formation of a spin-Peierls insulator state also exists in **1**.

3.7. Theoretical calculations

In order to explain the observed magnetic properties of **1**, a theoretical study was carried out. A methodology for magnetic molecular crystals, following the published procedure, was used [27]. Different pairs of paramagnetic molecules were chosen from the crystallographic data, selecting the more relevant interactions, taking into account that the magnetic exchange interaction, J_{AB}, varies inversely with the distance. 12 different pairs were studied, the results showed that only 7 values of intermolecular J_{AB} are relevant, see Table 4.

First of all, the fragments: TCNQ$^-$ and *trans*-[Cr(cyclam)Cl$_2$]$^+$ were studied separately. In the TCNQ$^-$ it was found that the HOMO is an antibonding π orbital, delocalized mainly in the aromatic ring. Thus, the possible magnetic exchange interactions are favored in the central part of the ring. A similar analysis of the molecular orbitals of the cation *trans*-[Cr(cyclam)Cl$_2$]$^+$ showed that the HOMO is localized mainly over the Cl$^-$, exhibiting a strong p character. On the other hand, H_2O presented a lower orbital contribution and therefore, this molecule does not contribute significantly to the total magnetic exchange interaction.

The magnetic exchange interactions were obtained by means of the Heissenberg-Dirac-Van Vleck Hamiltonian:

$$\hat{H} = -2J_{AB}\hat{S}_A\hat{A}\cdot\hat{S}_B \qquad (2)$$

The main values of J_{AB} of the seven pairs are listed in Table 4. These calculations were made taking into account the closest distances of eclipsed atoms, e.g. C15–C20 (3.12 and 3.40 Å) of the alternating TCNQ neighbors. These values indicated that the TCNQ pair (d1) presents a very high antiferromagnetic exchange coupling J_{AB} via strong π–π interactions, making this pair a diamagnetic dimer. So, these diamagnetic dimers do not contribute to the total magnetic moment of the compound. In fact, most of the remaining studied pairs presented antiferromagnetic coupling, except the d_3 pair which exhibited a ferromagnetic interaction. These magnetic exchange couplings can be visualized through CH–π, Cl–π and hydrogen bonding [Fig. 14].

On the other hand, the results from the *trans*-[Cr(cyclam)Cl$_2$]$^+$ and TCNQ$^-$ alone resulted in a $S = 3/2$ and $S = 1/2$ ground state respectively. However, as these theoretical results confirmed, the TCNQ$^-$ units are grouped as diamagnetic dimers (Fig. 14a) and do not contribute to the paramagnetism of *trans*-[Cr(cyclam)Cl$_2$]

Table 4
Distances and exchange interaction values (J_{AB}) for the different pairs.

Pair		Distance (Å)	J_{AB} (K)
(d1)	TCNQ...TCNQ	3.12	−2137.49
(d2)	CrcyCl$_2$...TCNQ	2.70	−0.26
(d_3)	CrcyCl$_2$...TCNQ	2.36	0.69
(d_4)	CrcyCl$_2$...TCNQ	2.88	−0.42
(d_5)	CrcyCl$_2$...TCNQ	2.55	−0.26
(d_6)	Crcy·H2O...TCNQ	2.69	−0.27
(d_7)	Crcy·H2O...TCNQ	2.70	−0.29

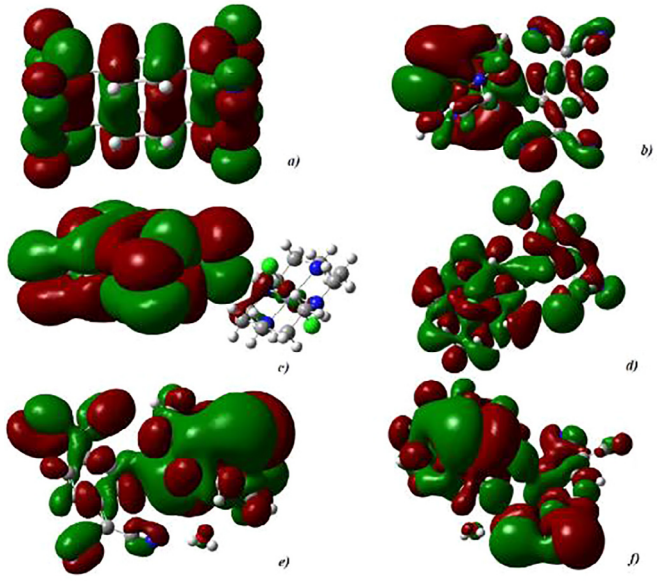

Fig. 14. MO's of the pairs: (a) HOMO of d1, (b) FOMO 135 of d2, (c) HOMO of d3, (d) FOMO 121 of d4, (e) FOMO 135 of d6, f) FOMO 135 of d7.

TCNQ, finding that only the *trans*-[Cr(cyclam)Cl_2]$^+$ cation is the responsible for the observed paramagnetism. As a result, the van der Waals, CH–π, Cl–π and the N–H hydrogen bonding are originating the observed antiferromagnetism ($\theta = -15.38$ K) in **1**.

4. Conclusions

The reaction between the pinkish *trans*-[Cr(cyclam)Cl_2]Cl and LiTCNQ produced the very dark purple *trans*-[Cr(cyclam)Cl_2]TCNQ·H_2O compound, which structure consists of a *trans* dichloro cyclam chromium cation [Cr(*RSSR*-cyclam)Cl_2]$^+$, a $TCNQ^-$ anion and a water solvent molecule. The crystalline array showed that the molecules of $TCNQ^-$ anions in compound **1** are stacked into columns along the b axis with alternating distances (3.24 and 3.87 Å), through strong π–π interactions. This stacking favors the free movement of the conduction electrons through the columns of $TCNQ^-$, causing the semiconductor behavior of **1,** for which the measured conductivity was $\sigma_{298K} = 1.94 \times 10^{-5}$ Scm^{-1} and its band gap of 0.53 eV is well in the range of the semiconductors.

1 shows a typical Curie–Weiss behavior at variable temperature. Its magnetic moment at room temperature $\mu_{exp} = 3.84$ B. M. is lower than the expected $\mu_{calc} = 4.86$ B. M. DFT calculations show a strong antiferromagnetic interaction between $TCNQ^-$ molecules, causing pairing of the electrons, which lead to the formation of stable diamagnetic dimers with a strong exchange interaction of $J = -2137.49$ K. This is consistent with the EPR spectrum where no radical signal from $TCNQ^-$ is observed. Thus, the exhibited magnetic moment of $\mu_{exp} = 3.84$ B. M. for *trans*-[Cr(cyclam)Cl_2]TCNQ·H_2O lower than the expected value for 4 unpaired electrons, $\mu_{calc} = 4.86$ B. M. can be explained by the good overlap of the HOMO's orbitals of the $TCNQ^-$ along the *b* axis through π–π stacking. The antiferromagnetic coupling, $\theta = -15.38$ K found for this compound, was rationalized with van der Waals, CH–π, Cl–π and hydrogen bonding interactions.

The broad band centered at 840 nm in the emission spectrum of **1**, was attributed to the $^4T_{2g} \rightarrow {}^4A_{2g}$ transition of Cr(III). Unexpectedly, no sharp bands from the $^2T_{1g}$ and ^2E_g levels were observed under these conditions.

As a general conclusion, a multifunctional molecular material, **1**, has been obtained by the combination of two selected molecular blocks, specifically *trans*-[Cr(cyclam)Cl_2]$^+$ and $TCNQ^-$. The magnetic and photoluminescence properties are originated in the Cr^{3+} cation. In counterpart, $TCNQ^-$ allowed **1** to have the semiconducting properties, which could possibly be explored in the field of optoelectronics.

Acknowledgements

We gratefully acknowledge the financial support of CONACyT (México), Project 128921, J.P.L.G. thanks for the PhD scholarship 378482. DGAPA-UNAM, Project IT100217 and finally to the supercomputing facilities, LANCAD-UNAM-DGTIC-315. We also thank to V. H. Lemus Neri, N. Lopez Balbiaux and M. Gutierrez Franco from USAII-UNAM (Unidad de Servicios de Apoyo a la Investigación, Facultad de Química, UNAM) for their analytical services and technical assistance; S. Barragán Rosendo from Departamento de Diseño y Medios Audiovisuales FQ-UNAM; to Nicolas Bélanger-Desmarais for measuring the Raman spectra and to Dr. Miguel Castro for the revision of the theoretical calculations.

Appendix A. . Supplementary data

CCDC 1547475 contains the supplementary crystallographic data for *trans*-[Cr(*RSSR*-cyclam)Cl_2]TCNQ·H_2O. These data can be obtained free of charge via http://www.ccdc.cam.ac.uk/conts/retrieving.html, or from the Cambridge Crystallographic Data Centre, 12 Union Road, Cambridge CB2 1EZ, UK; fax: (+44) 1223-336-033; or e-mail: deposit@ccdc.cam.ac.uk.

References

[1] L. Ouahab (Ed.), Multifunctional Molecular Materials, Pan Stanford Publishing, USA, 2013.
[2] (a) R. Maurice, C. de Graaf, N. Guihéry, Phys. Chem. Chem. Phys. 15 (2013) 18784;
(b) E. Coronado, M. Yamashita, Dalton Trans. 45 (2016) 16553;
(c) H. Ohno, Nature Materials 9 (2010) 952;
(d) J. Camarero, E. Coronado, J. Mater. Chem. 19 (2009) 1678;
(e) D. Stepanenko, M. Trif, D. Loss, Inorg. Chim. Acta 361 (2008) 3740;
(f) A. Fert, Thin Solid Films 517 (2008) 2.
[3] (a) S.A. Wolf, D.D. Awschalom, R.A. Buhrman, J.M. Daughton, S. von Molnár, M. L. Roukes, A.Y. Chtchelkanova, D.M. Treger, Science 234 (2001) 1488;
(b) L. Ouahab, Coord. Chem. Rev. 178–180 (1998) 1501;
(c) E. Coronado, M. Clemente-León, J.R. Galán-Mascarós, C. Giménez-Saiz, C.J. Gómez-García, E. Martínez-Ferrero, J. Chem. Soc. Dalton Trans. (2000) 3955;
(d) E. Coronado, Peter Day, Chem. Rev. 104 (2004) 5419.
[4] (a) S. Decurtins, Phil. Trans. R. Soc. Lond. A 357 (1999) 3025;
(b) N. Hanasaki, H. Tajima, M. Matsuda, T. Naito, T. Inabe, Phys. Rev. B 62 (2000) 5839;
(c) E. Coronado, J.R. Galán-Mascarós, J. Mater. Chem. 15 (2005) 66;
(d) Y. Einaga, J. Photochem. Photobiol. C: Photochem. Rev. 7 (2006) 69;
(e) C. Atmani, F. El Hajj, S. Benmansour, M. Marchivie, S. Triki, F. Conan, V. Patinec, H. Handel, G. Dupouy, C.J. Gómez-García, Coordination Chemistry Reviews 254 (2010) 1559;
(f) N. Sabbatini, M. Guardigli, I. Manet, Handbook of the Physics and Chemistry of Rare Earths, ElSevier 23 (1996).
[5] (a) D. Gatteschi, L. Bogani, A. Cornia, M. Mannini, L. Sorace, R. Sessoli, Solid State Sci. 10 (2008) 1701;
(b) J.V. Yakhmi, Physica B 321 (2002) 204;
(c) A. Caneschi, D. Gatteschi, R. Sessoli, P. Rey, Acc. Chem. Res. 22 (1989) 392;
(d) E. Coronado, L.R. Falvello, J.R. Galán-Mascarós, C. Giménez-Saiz, C.J. Gómez-García, V.N. Laukhin, A. Pérez-Benítez, C. Rovira, J. Veciana, Adv. Mater. 9 (1997) 984;
(e) D. Amabilino, J. Cirujeda, J. Veciana, Phil. Trans. R. Soc. Lond. A 357 (1999) 2873;
(f) J.S. Miller, A.J. Epstein, W.M. Reiff, Science 240 (1988) 40;
(g) W. Fujita, K. Awaga, Science 286 (1999) 261.
[6] (a) A.A. Talin, A. Centrone, A.C. Ford, M.E. Foster, V. Stavila, P. Haney, R.A. Kinney, V. Szalai, F.E. Gabaly, H.P. Yoon, F. Léonard, M.D. Allendorf, Science 343 (2014) 66;
(b) M.R. Saber, A.V. Posvirin, B.F. Abrahams, R.W. Elliott, R. Robson, K.R. Dunbar, Chem. Eur. J. 20 (2014) 7593;
(c) W. Kaim, M. Moscherosch, Coord. Chem. Rev. 129 (1994) 157;
(d) S.A. Chavan, J.V. Yakhmi, I.K. Gopalakrishnan, Mater. Sci. Eng. C 3 (1995) 175;
(e) L.R. Melby, R.J. Harder, W.R. Hertler, W. Mahler, R.E. Benson, W.E. Mochel, J. Am. Chem. Soc. 84 (1962) 3374;
(f) J.S. Miller, D.T. Glatzhofer, D.M. ÓHare, W.M. Reiff, A. Chakraborty, A.J. Epstein, Inorg. Chem. 28 (1989) 2930.
[7] a) A. Nafady, A.P. ÓMullane, A.M. Bond, Coord. Chem. Rev. 268 (2014) 101;
b) C. Avendano, Z. Zhang, A. Ota, H. Zhao, K.R. Dunbar, Angew. Chem., Int. Ed. 50 (2011) 6543;
c) R.P. Shibaeva, L.O. Atovmyan, Zhurnal Strukturnoi Khimii 13 (1972) 546.
[8] (a) E.I. Kamitsos, W.M. Risen Jr., Solid State Commun. 45 (1983) 165;
(b) R.S. Potember, T.O. Poehler, R.C. Benson, Appl. Phys. Lett. 41 (1982) 548;
(c) B. Mukherjee, M. Mukherjee, K. Sim, S. Pyo, J. Mater. Chem. 21 (2011) 1931.
[9] T. Tiedje, J.F. Carolan, A.J. Berlinsky, L. Weiler, Can. J. Phys. 53 (1975) 1593.
[10] (a) Y.N. Shvachko, D.V. Starichenko, A.V. Korolyov, E.B. Yagubskii, A.I. Kotov, L. I. Buravov, K.A. Lissenko, V.N. Zverev, S.V. Simonov, L.V. Zorina, O.G. Shakirova, L.G. Lavrenova, Inorg. Chem. 55 (2016) 9121;
(b) Z. Chen, B. Zhao, P. Cheng, X.Q. Zhao, W. Shi, Y. Song, Inorg. Chem. 48 (2009) 3493.
[11] (a) A.J. Epstein, E.M. Conwell, Solid State Commun. 24 (1977) 627;
(b) R.L. Green, G.B. Street, Sci. New Series 226 (1984) 651.
[12] W.E. Broderick, B.M. Hoffman, J. Am. Chem. Soc. 113 (1991) 6334.
[13] W.E. Broderick, J.A. Thompson, E.P. Day, B.M. Hoffman, Science 249 (1990) 401.
[14] K. Ueda, T. Sugimoto, S. Endo, N. Toyota, M. Kohama, K. Yamamoto, Y. Suenaga, H. Morimoto, T. Yamaguchi, M. Munakata, N. Hosoito, N. Kanehisa, Y. Shibamoto, Y. Kai, Chem. Phys. Lett. 261 (1996) 295.
[15] G.A. Candela, L.J. Swartzendruber, J.S. Miller, M.J. Rice, J. Am. Chem. Soc. 101 (1979) 2755.
[16] E.B. Vickers, T.D. Selby, M.S. Thorum, M.L. Taliaferro, J.S. Miller, Inorg. Chem. 43 (2004) 6414.
[17] (a) R.P. Shibaeva, L.O. Atovmyan, L.P. Rozenberg, Chem. Comm. (1969) 649;
(b) R.P. Shibaeva, L.O. Atovmyan, M.N. Orfanova, Chem. Comm. (1969) 1494;
(c) A.R. Siedle, G.A. Candela, T.F. Finnegan, Inorg. Chim. Acta 35 (1979) 125.
[18] a) J. Nishijo, M. Enomoto, Inorg. Chim. Acta 437 (2015) 59;
b) J. Nishijo, Polyhedron 66 (2013) 43.

[19] (a) M. Flores-Alamo, M.E. Sosa-Torres, R.A. Toscano, E. Camarillo, J.M. Hernández, H. Murrieta, Inorg. Chem. Comm. 7 (2004) 1087;
(b) M. Flores-Alamo, M.E. Sosa-Torres, A. Solano-Peralta, R. Escudero, R.A. Toscano, M. Castro, E. Camarillo, J.M. Hernández, H. Murrieta, Inorg. Chim. Acta 357 (2004) 4596;
(c) M.E. Sosa, M.L. Tobe, J. Chem. Soc. Dalton Trans. (1986) 427.
[20] G.A. Bain, J.F. Berry, J. Chem. Educ. 85 (2008) 532.
[21] (a) Bruker, SAINT and TWINABS in APEX2, Bruker AXS Inc, Madison, Wisconsin, USA, 2012;
(b) George M. Sheldrick, SHELXT – Integrated space-group and crystal structure determination, Acta Cryst. A71 (2015) 3;
(c) G.M. Sheldrick, Crystal structure refinement with SHELXL, Acta Cryst. C71 (2015) 3–8;
(d) C.B. Hübschle, G.M. Sheldrick, B. Dittrich, ShelXle: a Qt graphical user interface for SHELXL, J. Appl. Cryst. 44 (2011) 1281.
[22] M.J. Frisch, G.W. Trucks, H.B. Schlegel, G.E. Scuseria, M.A. Robb, J.R. Cheeseman, G. Scalmani, V. Barone, B. Mennucci, G.A. Petersson, H. Nakatsuji, M. Caricato, X. Li, H.P. Hratchian, A.F. Izmaylov, J. Bloino, G. Zheng, J.L. Sonnenberg, M. Hada, M. Ehara, K. Toyota, R. Fukuda, J. Hasegawa, M. Ishida, T. Nakajima, Y. Honda, O. Kitao, H. Nakai, T. Vreven, J.A. Montgomery Jr., J.E. Peralta, F. Ogliaro, M. Bearpark, J.J. Heyd, E. Brothers, K.N. Kudin, V.N. Staroverov, R. Kobayashi, J. Normand, K. Raghavachari, A. Rendell, J.C. Burant, S.S. Iyengar, J. Tomasi, M. Cossi, N. Rega, J.M. Millam, M. Klene, J.E. Knox, J.B. Cross, V. Bakken, C. Adamo, J. Jaramillo, R. Gomperts, R.E. Stratmann, O. Yazyev, A.J. Austin, R. Cammi, C. Pomelli, J.W. Ochterski, R.L. Martin, K. Morokuma, V.G. Zakrzewski, G.A. Voth, P. Salvador, J.J. Dannenberg, S. Dapprich, A.D. Daniels, Ö. Farkas, J.B. Foresman, J.V. Ortiz, J. Cioslowski, D.J. Fox, Gaussian 09, Revision D.01, Gaussian Inc, Wallingford CT, 2009.
[23] A.D. Becke, J. Chem. Phys. 98 (1993) 5648.
[24] B. Bosnich, C.K. Poon, M. Tobe, Inorg. Chem. 4 (1965) 1102.
[25] Frank DeRosa, Bu. Xianhui, Kristina Pohaku, Peter C. Ford, Inorg. Chem. 44 (2005) 4166.
[26] C. Kittel, Introduction to Solid State Physics, 8th ed., John Wiley & Sons, 2005.
[27] M. Deumal, M.A. Robb, J.J. Novoa, Theoretical study of the magnetism in molecular crystals using a first-principles bottom-up methodology, in: S. Lahmar, J. Maruani, S. Wilson, G. Delgado-Barrio (Eds.), Topics in the Theory of Chemical and Physical Systems. Progress in Theoretical Chemistry and Physics, Springer, Dordrecht, 2007, p. 271.